SAND2016-2548C

VCSELs for interferometric readout of MEMS sensors

Darwin K. Serkland*, Kent M. Geib, Gregory M. Peake, Gordon A. Keeler,
Michael J. Shaw, Michael S. Baker, and Murat Okandan†
Sandia National Laboratories, Albuquerque, NM 87185

ABSTRACT

We report on the development of single-frequency VCSELs (vertical-cavity surface-emitting lasers) for sensing the position of a moving MEMS (micro-electro-mechanical system) object with resolution much less than 1nm. Position measurement is the basis of many different types of MEMS sensors, including accelerometers, gyroscopes, and pressure sensors. Typically, by switching from a traditional capacitive electronic readout to an interferometric optical readout, the resolution can be improved by an order of magnitude with a corresponding improvement in MEMS sensor performance. Because the VCSEL wavelength determines the scale of the position measurement, laser wavelength (frequency) stability is desirable. This paper discusses the impact of VCSEL amplitude and frequency noise on the position measurement.

Keywords: VCSEL, MEMS, sensor, interferometer, linewidth, frequency noise, MEMS sensor, optical MEMS

1. INTRODUCTION

MEMS (micro-electro-mechanical system) sensors are emerging in commercial markets, often delivering similar or better performance than conventional sensors, but with significant reductions in package size, power consumption, and cost. Although MEMS sensors span a wide range of applications, including accelerometers, gyroscopes, microphones, and pressure sensors, they all fundamentally operate by measuring the position of a moving object. For example, as shown in Figure 1, a MEMS pressure sensor measures the position of a diaphragm which moves downward as the sensed pressure above the MEMS device increases. Historically, capacitive readout of the position of the moving element has been the most widely adopted readout technique, especially for commercial MEMS sensors. Again, considering the example sensor shown in Figure 1, the raw measurement is of capacitance between two parallel plates: the top plate attached to the moving diaphragm and the bottom plate fixed to the body of the MEMS device. If the external pressure (to be measured) increases the diaphragm moves downward, decreasing the gap between the parallel plates and causing the capacitance to increase. So measured capacitance is proportional to sensed pressure. Capacitive position sensors are attractive because they can be fabricated into the MEMS device with minimal additional cost, since they only require two conductive plates separated by a gap that is produced by the "release" process step. In this paper, we will consider how optical readout of position has the potential to improve MEMS sensor performance. The small size, low power consumption, and low cost of VCSELs (vertical-cavity surface-emitting lasers) make them natural candidates for optical readout of MEMS sensors.

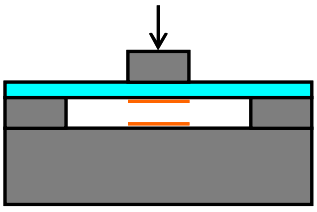

Figure 1. Schematic cross-sectional view of a MEMS pressure sensor. Increasing pressure outside the MEMS sensor, relative to the internal cavity pressure, drives the diaphragm downward as indicated by the direction of the arrow.

* DKSERKL@sandia.gov; phone: (505) 844-5355; fax: (505) 844-8985; http://www.sandia.gov/
† Current affiliation: EIOS, Inc., mokandan@gmail.com

2. POSITION READOUT: CAPACITIVE OR OPTICAL

In this section, we survey capacitive and optical position readout techniques in order to better understand the benefits and limitations of the various techniques. We start by considering capacitive readouts, which are essentially based on sensing the capacitance between two parallel conductive plates, as shown in Figure 2(a). A change in position of plate 1 with respect to a fixed plate 2 will change the capacitance between the two plates, according to the capacitance formula $C = \varepsilon_0 \varepsilon_r A / d$, where $A = LW$ is the area of overlap, d is the gap between the plates, $\varepsilon_0 = 8.85\text{pF/m}$ is the permittivity of vacuum, and ε_r is the relative permittivity of the medium between the plates ($\varepsilon_r = 1$ for vacuum and air). A vertical motion of plate 1, as shown in Figure 2(a), changes the gap between the plates and hence the capacitance. If the gap is nominally 1 μm, then a vertical movement of 0.1 μm changes the capacitance by 10%. The technique of measuring changes in the gap can be relatively sensitive to small motions, but the dynamic range is limited to the nominal gap distance. Moreover, the change in capacitance versus position is not linear, since capacitance changes as the inverse of the gap thicknesses.

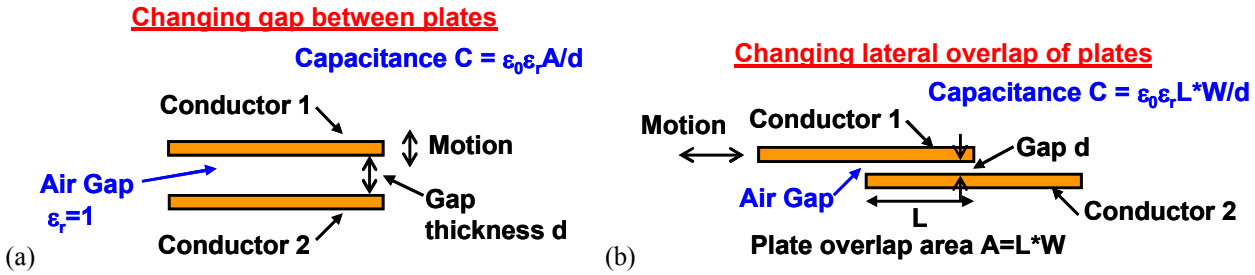

Figure 2. Capacitance between two parallel plates depends on the area A of overlap and the gap d between the plates. (a) Motion that changes the gap d between the plates can change the capacitance. (b) Motion that changes the area A=L*W of lateral overlap of the two plates also changes the capacitance.

Alternatively, rather than change the gap between two plates, one can change the area of overlap by moving one plate laterally relative to the other, as shown in Figure 2(b). A lateral motion of plate 1 changes the length L of overlap, thereby changing the area of overlap A=L*W, where W is the width of overlap between the two plates. As an example, if two plates of length L = 500 μm, width = 500 μm, and gap = 1 μm, are completely overlapped the capacitance is 2.2 pF, which is measurable with moderate resolution. Continuing the example, if plate 1 is moved laterally by 50 μm, then the length of overlap decreases to 450 μm and the capacitance decreases by 10% to 2.0 pF. Comparing our examples of lateral and vertical motion, the lateral capacitance sensor is 500 times less sensitive to changes in position but has 500 times larger dynamic range, being capable of measuring motion over the full range of 500 μm.

Next, we consider the lateral motion sensor shown schematically in Figure 3(a). Here two periodic arrays of conductive plates are used, where for example each plate in the array measures 2 μm long by 500 μm wide. The advantage of this configuration is that it regains much of the sensitivity that was lost in the previous lateral motion sensor, as shown by the capacitance versus position plot in Figure 3(b). The capacitance varies by almost 100% for a lateral motion of one half of the period, which for the example shown is only 2 times less sensitive than the vertical position sensor. And there is no loss of dynamic range of motion, provided we are capable of keeping track of the period within which we are positioned.

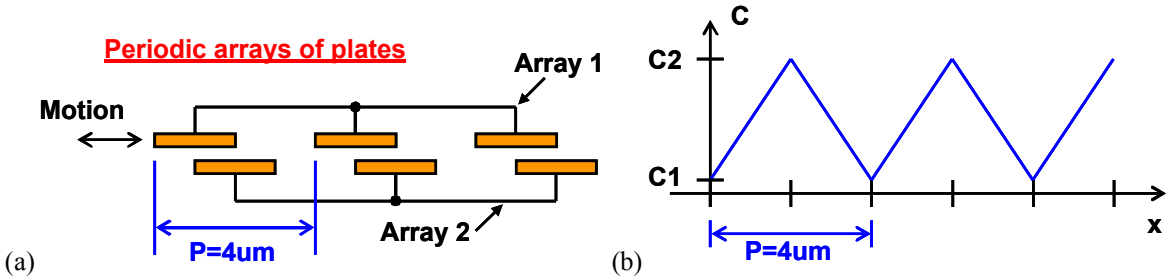

Figure 3. (a) Schematic cross-sectional view of two periodic arrays of conductive plates used for capacitive sensing of lateral motion. (b) Periodic variation of capacitance measured between the two arrays versus lateral position of array 1.

We note that the capacitance versus position plot of Figure 3(b) is only obtained for extremely thin gaps, whereas for a more realistic gap of 1 μm the saw-tooth waveform would exhibit rounded crests and valleys due to the fringing electric fields at the edges of the plates.

Next, we will consider optical readout techniques, focusing exclusively on interferometric configurations that provide high position sensitivity. We start by considering the classic Michelson interferometer, as shown schematically in Figure 4(a). In the Michelson interferometer, a single-frequency laser beam is split by a 50% transmission (50% reflection) beam splitter into two arms: transmitted and reflected. The laser beam in each arm is reflected by an end mirror at an angle near normal incidence. In the configuration shown, the end mirror in the transmitted arm is fixed, and the end mirror in the reflected arm is attached to a moving MEMS object. The retro-reflected beams recombine at the beam splitter, and emerge into two output ports: port P1 propagating toward the photodiode, and port P0 (which is often ignored) propagating toward the laser diode. Figure 4(b) shows the optical powers emerging from the two output ports P0 and P1 versus the position offset dz of the moving mirror, assuming a laser wavelength of 850 nm. The two signals vary as $\cos^2(\phi)$ and $\sin^2(\phi)$, where $\phi=2\pi*dz/\lambda$, and λ is the laser wavelength. The signals are sinusoidal with periodicity $\lambda/2 = 425$ nm.

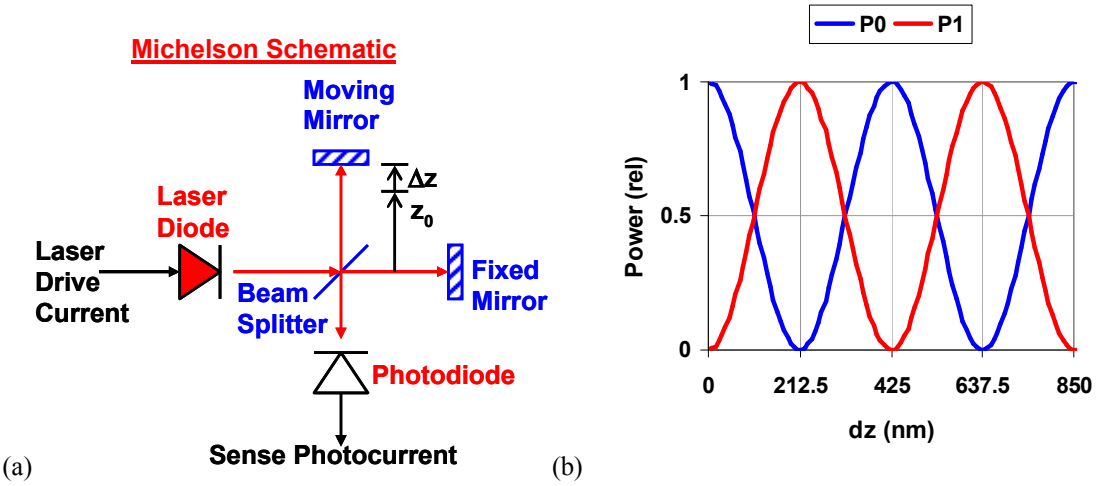

Figure 4. (a) Schematic drawing of a Michelson interferometer, showing a single-frequency laser diode, beam splitter, fixed and moving end mirrors, and photodiode to detect the output power from port P1. (b) Detected power at Michelson output ports P0 and P1 versus moving mirror displacement dz, assuming a laser wavelength of 850 nm.

The signals from the Michelson interferometer are similar to those from the array of capacitors, except the periodicity has been reduced by approximately an order of magnitude from 4 μm to $\lambda/2$=0.425 μm. Hence, the optical interferometer has approximately 10 times higher sensitivity than the capacitive sensor, assuming that the signal-to-noise ratios are comparable. Like the capacitor array, the Michelson interferometer accommodates a very large dynamic range of motion, easily exceeding 1 mm. The dynamic range of the Michelson interferometer is only limited by mode matching of the two laser beams that return to the beam splitter from the two arms of the interferometer. For equal length arms, the two return beams will be perfectly mode matched at the beam splitter. However, as the arm containing the moving mirror changes length, the reflected laser beam will change in diameter (and phase curvature) to the extent that the beam diverges (or converges) versus propagation distance. A collimated laser beam maintains a relatively constant beam diameter over a length scale on the order of one Rayleigh range $z_R = \pi w_0^2 / \lambda$, where w_0 is the beam waist (radius at $1/e^2$ intensity), and λ is the wavelength. For an example beam waist w_0 = 50 μm, the Rayleigh range z_R is 9 mm, which is a much longer distance than most MEMS parts can realistically move.

We have implemented a Michelson interferometer with a small mirror glued to a moving MEMS proof mass and demonstrated high contrast ratio fringes over a full range of MEMS motion of approximately 100 μm. The primary disadvantage of the Michelson interferometer configuration is the difficulty of integrating the beam splitter and the two end mirrors in a compact geometry that is easy to manufacture.

An alternative interferometer configuration that we call a "grating interferometer" is shown schematically in Figure 7(a).[1] Here we show a single-frequency VCSEL as the light source that illuminates a fixed grating reflector from above at an angle of incidence near 0 degrees. The fixed grating reflector by itself reflects light into several diffraction orders, but we show in Figure 7(a) only the lowest three diffraction orders (0, +1, -1) that are the most powerful. Half of the VCSEL light is transmitted through the slit openings in the diffraction grating and reflects from the moving mirror surface located a distance z below the top of the fixed grating. In practice, a metallic reflector layer (such as 100 nm of aluminum) is deposited onto the grating and moving mirror to make each surface reflectivity approach 100%. The light that reflects from the moving mirror and returns through the grating openings incurs a round-trip phase shift of $2\phi=4\pi*z/\lambda$, relative to the light that reflected from the top of the fixed grating, and also is diffracted into several orders. The two beams (reflected and transmitted) that emerge into each diffraction order interfere according to their relative phase shift 2ϕ. Figure 7(b) shows the power detected in the 0^{th} and 1^{st} ($P_{+1} + P_{-1}$) diffraction orders versus displacement z of the moving mirror, assuming a laser wavelength of 850 nm. The two signals vary as $P_0 = P_{in}*\cos^2(\phi)$ and $P_{-1} = P_{+1} = P_{in}*(4/\pi^2)*\sin^2(\phi)$, where $\phi=2\pi*z/\lambda$, and λ is the laser wavelength. The signals are sinusoidal with periodicity $\lambda/2 = 425$ nm, the same as for the Michelson interferometer.

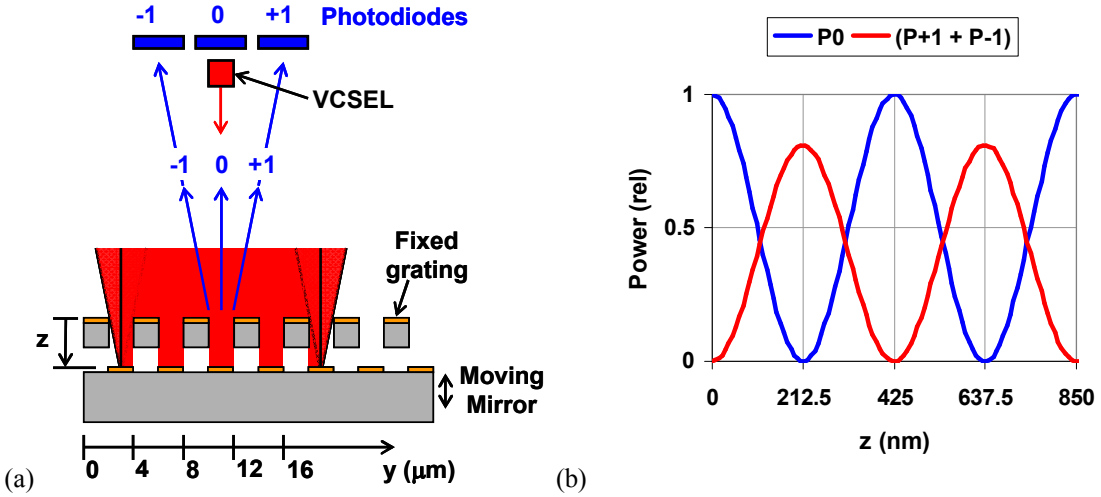

Figure 5. (a) Schematic cross-sectional drawing of the grating interferometer, showing a single-frequency VCSEL, fixed grating reflector, moving MEMS reflector, and three photodiodes to detect the diffracted orders: -1, 0 , +1. (b) Detected power in the 0^{th} and 1^{st} diffraction orders versus moving mirror displacement z, assuming a laser wavelength of 850 nm.

We describe the operation of the grating interferometer heuristically as follows. First, consider what would happen if the moving mirror reflectors were displaced upward, referring to the geometry of Figure 7(a), to the same level as the reflectors on the surface of the fixed grating. In that case, z = 0 nm and a single flat mirror surface is achieved, which reflects 100% of the light into the so-called 0-order spot and no light is reflected into higher diffraction orders. Next consider what happens when the moving mirror is displaced by a quarter wavelength to z = 212.5 nm, such that the light transmitted through the openings in the grating returns with a 180-degree phase shift. Now 50% of the beam reflects from the grating surface with 0-degree phase shift and 50% of the beam returns from the moving mirror with 180-degree phase shift, yielding complete destructive interference into the 0-order spot. Since conservation of energy always applies, we conclude that the incident optical power must be directed into the higher-order diffraction spots, most (81%) going into the first-order spots.

The grating interferometer is topologically equivalent to the Michelson interferometer and achieves the same sensitivity but in a much more compact geometry. However, the grating interferometer does reduce the dynamic range of MEMS motion. The limitation on dynamic range arises due to diffraction of light transmitted through the grating slits. Ideally the light transmitted through each slit opening in the grating would not spread laterally and therefore would all return back through the slit after reflecting from the surface of the moving mirror. In reality, the narrower the slit opening in the grating, the more the transmitted light will diffract and spread laterally before returning back through the slit opening. Any return light that has spread beyond the slit opening width will be clipped by the grating fingers and

therefore reduce interferometer fringe contrast. Increasing the grating period and hence the slit width will reduce the clipping of transmitted light and enable a larger dynamic range of MEMS motion.

We have previously developed monolithically integrated VCSELs and resonant-cavity photodiodes (RCPDs) fabricated from a single VCSEL epitaxial stack that yielded all of the required optoelectronic capabilities in a single chip, as shown in Figure 6(a).[2] The use of such an integrated VCSEL-detector chip yields the smallest possible form factor for implementing the grating interferometer. Without using a collimating lens, the beam diameter on the grating depends on the VCSEL divergence angle and the distance from the VCSEL to the grating. Also, the optical feedback into the VCSEL depends on the distance to the grating and the VCSEL divergence angle, assuming that the two parts are not tilted with respect to each other by more than the VCSEL divergence angle.

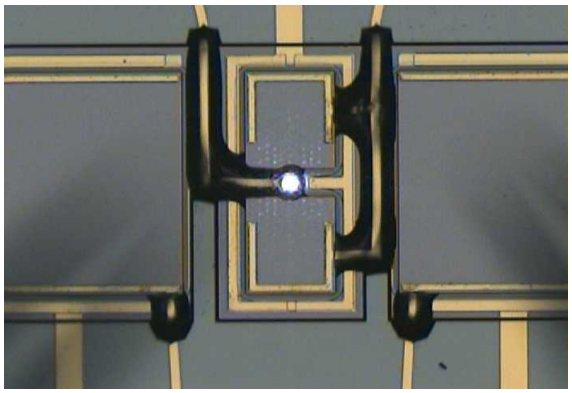

Figure 6. Monolithically integrated VCSEL and 3 resonant-cavity photodiodes (RCPDs) that provide all of the optoelectronic capabilities required for the grating interferometer implementation.

3. VCSELS FOR INTERFEROMETRIC POSITION READOUT

In this section we will discuss the requirements that VCSELs must meet for use in MEMS interferometric position readouts. We will show measured data obtained with a VCSEL and a MEMS interferometer. At the end of this section we will discuss the impact of VCSEL intensity noise and frequency noise on the position measurement resolution. As a general observation, we note that the VCSEL requirements for MEMS interferometry are similar to those for atomic spectroscopy. Figure 7(a) shows an optical micrograph of a lasing VCSEL that we have developed for MEMS interferometry, which is very similar to the narrow-linewidth VCSELs that we have previously developed for atomic clocks.[3] Figure 7(b) shows the measured output optical power and voltage drop versus input current.

(a)

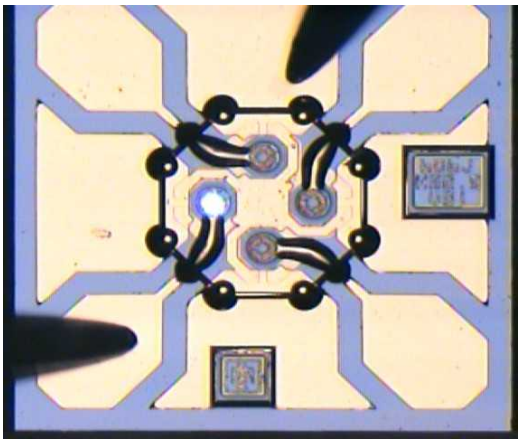

(b)

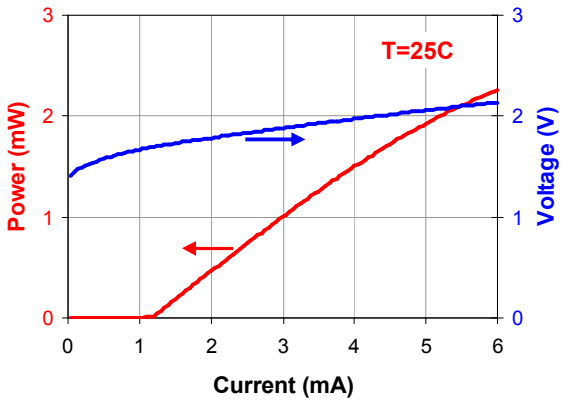

Figure 7. (a) Photograph of a single-frequency VCSEL, driven with 2mA current . (b) VCSEL output optical power and voltage drop versus current.

One of the most important requirements for interferometry is that the VCSEL should operate in a single frequency mode. Figure 8(a) shows the single-frequency 855-nm emission spectrum of our VCSEL at a drive current of 3 mA, exhibiting a side-mode suppression ratio is 33 dB. This VCSEL had an oxide aperture diameter of 4.0 μm, and operated in a single mode (single frequency and single linear polarization) over the full range of currents that we tested (up to 6 mA). Figure 8(b) shows the 10.5 MHz linewidth measured from another VCSEL of the same design. The linewidth was measured by coherently combining the VCSEL output with the output of an external-cavity diode laser (specified to have linewidth less than 1 MHz), and detecting the resulting radio-frequency beat note with a 12-GHz-bandwidth photodetector (New Focus model 1580-B) and a spectrum analyzer.[3]

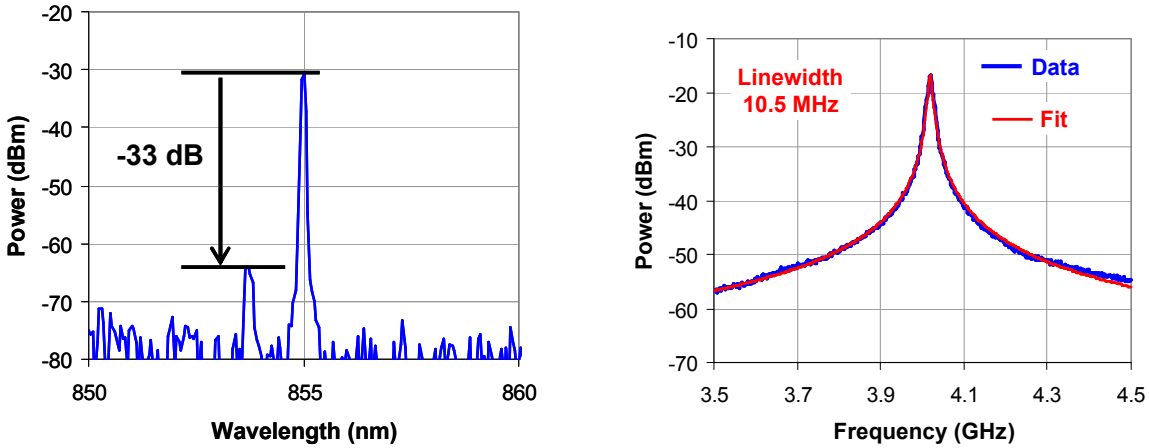

(a) (b)

Figure 8. (a) Single mode emission spectrum of the VCSEL, measured at a drive current of 3 mA. (b) Heterodyne linewidth measurement of a similar narrow-linewidth VCSEL exhibiting a 10.5 MHz linewidth.

We used the collimated output from our single-frequency VCSEL to drive a grating interferometer like the one shown in Figure 9(a). The fixed grating of pitch 4 μm was fabricated by etching a layer of polysilicon, producing a 100 μm square grating suspended above a moveable silicon proof mass. The proof mass was electrostatically driven in the vertical direction by applying a saw-tooth waveform (Vin) shown in Figure 9(b). The motion of the proof mass was measured by detecting the optical powers in the +0 (PO) and +1 (P+1) diffraction orders, as shown in Figure 9(b). As expected, the signals P0 and P+1 are out of phase, and we know that the distance from valley to crest is $\lambda/4 = 213$ nm.

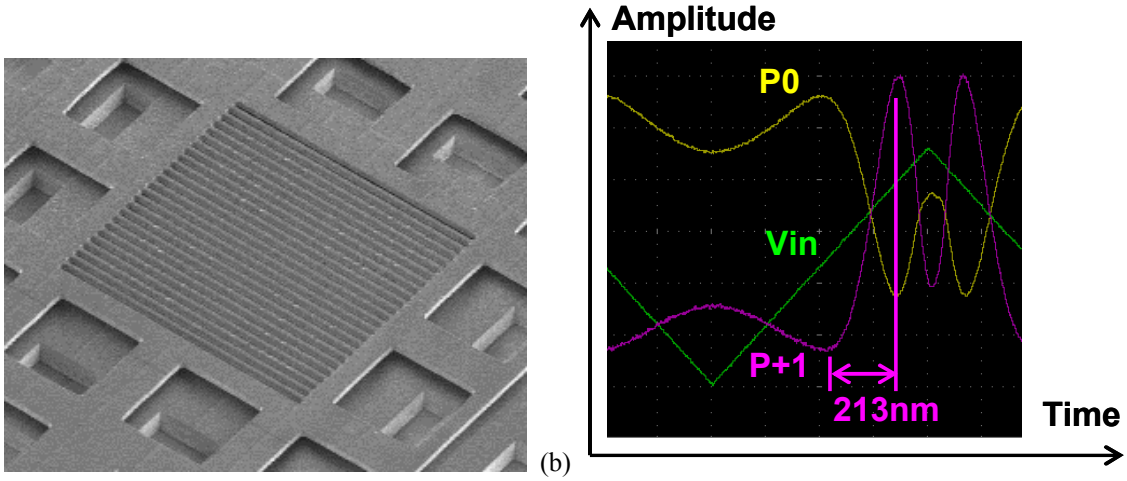

(a) (b)

Figure 9. (a) Silicon MEMS grating of pitch 4 μm, measuring 100 μm square, suspended above a moving silicon proof mass. (b) Measured power reflected into diffraction orders 0 (PO) and +1 (P+1) versus time as the MEMS proof mass was driven electrostatically by the saw-tooth waveform Vin.

It is clear from the oscilloscope data shown in Figure 9(b) that the signal-to-noise ratio obtained with our VCSEL was reasonably high (greater than 40 dB in a 1 MHz detector bandwidth). The interferometric readout is most sensitive on the linear part of the fringe waveform. At this operating point the position uncertainty δz is related to the signal amplitude uncertainty δs (measured relative to the full fringe amplitude) by the equation $\delta z = \delta s * \lambda/(4\pi) = \delta s * 68$ nm. Hence, a change in detected optical power of $\delta s = 0.01$ (relative to the full fringe amplitude) corresponds to a displacement of 0.68 nm. We can also use this equation to determine the minimum resolvable motion δz_{min} from a knowledge of the amplitude signal-to-noise ratio (SNR) as $\delta z_{min} = 68$ nm / SNR. As an example, a realistic signal-to-noise ratio of 100 dB yields an amplitude SNR = $1*10^5$ and so $\delta z_{min} = 0.68$ pm. Since single-mode VCSELs can readily achieve relative intensity noise (RIN) values of -140 dB/Hz, they will achieve a 100 dB signal-to-noise ratio in a bandwidth of 10 kHz.[4]

Finally, we consider the effect of VCSEL frequency noise on the minimum detectable displacement δz_{min}. To this end, we consider the Michelson interferometer shown in Figure 10, which has arm lengths L_1 and L_2. We define the difference in the arm lengths of the interferometer as $L = L_2 - L_1$. For equal arm lengths $L = 0$ and the interferometer output is insensitive to changes in the VCSEL frequency. For this reason the equal-arm-length interferometer is known as a "white light" interferometer that can produce fringes even with broad-spectrum illumination. However, typical MEMS interferometers do not have equal arm lengths, and hence the output power detected by the photodiode will change if the VCSEL frequency changes. We can quantify this statement by noting that a change in VCSEL frequency δf will produce a differential phase change in the two arms of $\delta\phi = 4\pi*(L/\lambda)*(\delta f/f)$, where f is the (optical) frequency of the VCSEL. For a VCSEL wavelength $\lambda = 850$ nm (frequency f = 353 THz), and a difference in arm lengths L = 10 μm, a VCSEL frequency uncertainty of $\delta f = 50$ MHz corresponds to a position uncertainty of $\delta z_{min} = 1.4$ pm.

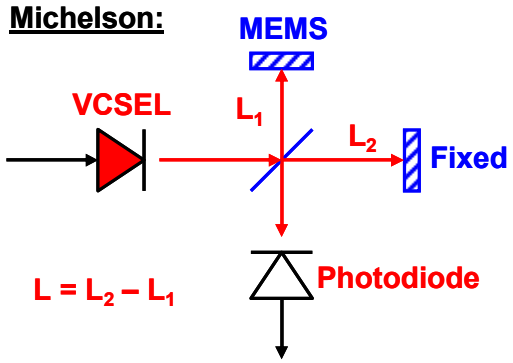

Figure 10. Michelson interferometer with arm lengths L_1 and L_2. We define the difference length $L = L_2 - L_1$.

The grating interferometer described in the previous section is equivalent to the Michelson interferometer with an arm length difference L equal to the distance from the top of the grating to the top of the moving mirror. For the example, the grating interferometer shown previously in Figure 9(a) had an arm length difference of L = 5 μm. It is clear that all grating interferometers have an arm length difference of at least a few microns and are correspondingly susceptible to frequency noise of the VCSEL. Thus, there is a clear benefit to using VCSELs with narrow linewidths.

4. CONCLUSIONS

In conclusion, interferometric readout of MEMS sensors has the potential to improve the position detection limit by an order of magnitude relative to conventional capacitive readouts. The small size, low power consumption, and low cost of VCSELs make them natural candidates for optical readout of MEMS sensors. However, interferometric readouts require single-mode (single frequency and single polarization) VCSELs for stable low-noise performance. Moreover, the VCSEL should have low intensity noise and low frequency noise in order to achieve the lowest uncertainty in the readout of the MEMS position. We have fabricated single-mode VCSELs with relative intensity noise of -140 dB/Hz and linewidths of 10 MHz that are well suited for the readout of interferometric MEMS sensors.

ACKNOWLEDGMENTS

The authors wish to thank V. M. Sanchez, S. Parameswaran, and T. M. Bauer for their expert technical assistance. Sandia National Laboratories is a multi-program laboratory managed and operated by Sandia Corporation, a wholly owned subsidiary of Lockheed Martin Corporation, for the U.S. Department of Energy's National Nuclear Security Administration under contract DE-AC04-94AL85000.

REFERENCES

[1] N. A. Hall, W. Lee, and F. L. Degertekin, “Capacitive Micromachined Ultrasonic Transducers with Diffraction-Based Integrated Optical Displacement Detection,” IEEE Trans. Ultrason., Ferroelectr., Freq. Control, vol. 50, pp. 1570-1580 (2003).

[2] N. A. Hall, M. Okandan, R. Littrell, D. K. Serkland, G. A. Keeler, K. Peterson, B. Bicen, C. T. Garcia, and F. L. Degertekin, “Micromachined Accelerometers With Optical Interferometric Read-Out and Integrated Electrostatic Actuation,” J. Microelectromech. Syst., vol. 17, pp. 37-44 (2008).

[3] D. K. Serkland, G. A. Keeler, K. M. Geib, and G. M. Peake, " Narrow Linewidth VCSELs for High-Resolution Spectroscopy," Proc. SPIE, vol. 7229, article 722907 (2009).

[4] R. Littrell, N. A. Hall, M. Okandan, R. Olsson, and D. Serkland, “Impact of relative intensity noise of vertical-cavity surface-emitting lasers on optics-based micromachined audio and seismic sensors,” Appl. Optics, vol. 46, pp. 6907-6911 (2007).